ACS Chemical Neuroscience

Research Article

pubs.acs.org/chemneuro

Functionalized Fullerene Targeting Human Voltage-Gated Sodium Channel, $hNa_v1.7$

Tamsyn A. Hilder,*[†,‡] Anna Robinson,[‡] and Shin-Ho Chung[‡]

[†]School of Chemical and Physical Sciences, Victoria University of Wellington, Wellington 6040, New Zealand

[‡]Computational Biophysics Group, Research School of Biology, Australian National University, Acton, ACT 2601, Australia

Supporting Information

ABSTRACT: Mutations of $hNa_v1.7$ that cause its activities to be enhanced contribute to severe neuropathic pain. Only a small number of $hNa_v1.7$ specific inhibitors have been identified, most of which interact with the voltage-sensing domain of the voltage-activated sodium ion channel. In our previous computational study, we demonstrated that a $[Lys_6]$-C_{84} fullerene binds tightly (affinity of 46 nM) to Na_vAb, the voltage-gated sodium channel from the bacterium *Arcobacter butzleri*. Here, we extend this work and, using molecular dynamics simulations, demonstrate that the same $[Lys_6]$-C_{84} fullerene binds strongly (2.7 nM) to the pore of a modeled human sodium ion channel $hNa_v1.7$. In contrast, the fullerene binds only weakly to a mutated model of $hNa_v1.7$ (I1399D) (14.5 mM) and a model of the skeletal muscle $hNa_v1.4$ (3.7 mM). Comparison of one representative sequence from each of the nine human sodium channel isoforms shows that only $hNa_v1.7$ possesses residues that are critical for binding the fullerene derivative and blocking the channel pore.

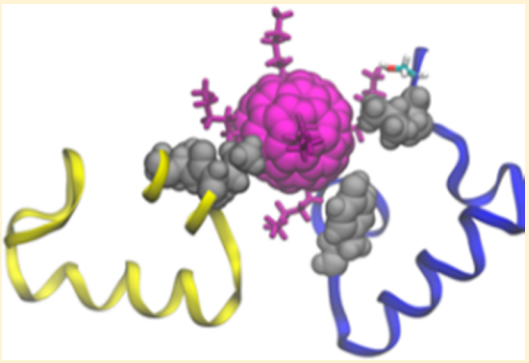

KEYWORDS: *Human voltage-gated sodium channel ($hNa_v1.7$), fullerenes, molecular dynamics, channel blocker, pain therapy*

INTRODUCTION

Chronic pain affects approximately 20% of the adult population.[1] Despite the significant economic cost of chronic pain, estimated to be approximately $600 billion per annum in the United States,[1] research into possible therapeutic compounds is still in early stages.[2] There is a genuine need to find therapeutic compounds for the treatment of chronic pain as current analgesics are restricted by problems such as dose-limiting side effects, tolerance, and potential for addiction.[1]

Voltage-gated sodium channels (VGSCs) are the primary mediators of electrical signal amplification and propagation in excitable cells.[3,4] Mammalian VGSCs are polypeptides of ~2000 amino acids in length and are comprised of an α-subunit with 2 auxiliary β-subunits. The α-subunit inserts into membranes in a conserved structural motif of 24 transmembrane helices configured into four distinct homologous repeats, designated Domains I–IV.[4−6] Each of the four domains is composed of six transmembrane helices (S1–S6) joined by cytoplasmic and extracellular loops of variable composition and length. Helices S1–S4 form the voltage sensing module. Helices S5 and S6 are connected by two short helical peptides (P1 and P2) and a selectivity filter (SF) loop which together form the outer vestibule and ion permeation pore. Sodium channels are molecular targets for a broad range of naturally occurring neurotoxins. These toxins have been extensively researched and shown to interact at known ion channel receptor sites (see Figure 1).[7]

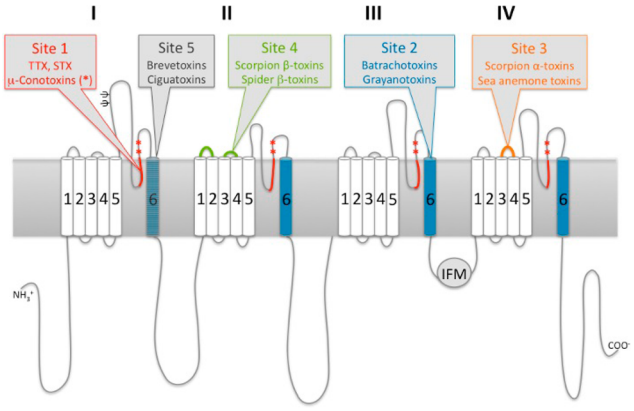

Figure 1. Schematic two-dimensional representation for each of the domains (I–IV) of the functional α-subunit of voltage-gated sodium channels and identification of known neurotoxin binding sites. Highlighted in red is the selectivity filter and entrance to the pore. This site is also the location of binding for tetrodotoxin (TTX), saxitoxin (STX), μ-conotoxins, as well as the $[Lys_6]$-C_{84} fullerene described here. Reproduced with permission from ref 7.

Genetic, structural, and functional studies have shown that the voltage-gated sodium channel, $hNa_v1.7$, contributes to pain

Received: March 14, 2017
Accepted: May 18, 2017
Published: June 6, 2017

DOI: 10.1021/acschemneuro.7b00099
ACS Chem. Neurosci. 2017, 8, 1747−1755

disorders. A gain-of-function mutation of this channel leads to severe neuropathic pain, whereas loss-of-function mutations lead to an indifference to pain.[8] Humans lacking this channel are completely insensitive to pain.[1] Therefore, selective inhibitors of $hNa_v1.7$ ion channels offer a new approach in the design of analgesics for treating a broad range, but not all,[2] of pain conditions.[9,10]

For an inhibitor of $hNa_v1.7$ to be of potential therapeutic value, it should have isoform-selectivity.[2] There are nine human Na_v channel isoforms, defined by differences in the sequences of the α-subunits. They are associated with migraine ($hNa_v1.1$), epilepsy ($hNa_v1.1-1.3$, $hNa_v1.6$), pain ($hNa_v1.7-1.9$), cardiac ($hNa_v1.5$), and muscle paralysis ($hNa_v1.4$) syndromes.[11] The high degree of amino acid sequence homology among the different isoforms makes finding subtype-selective ligands extremely difficult.[4] Blockers of hNa_v channels can be used to treat many neurological and cardiovascular disorders, but therapeutic utility is limited when isoform-selectivity is limited or absent. Successful blockers need to be designed to take advantage of subtle amino acid sequence variations in and around the pore region.

Due to their therapeutic potential, interest in identifying inhibitors of $hNa_v1.7$ is increasing. Most of the inhibitors of $hNa_v1.7$ discovered to date act by interacting with the voltage-sensor.[9,11−16] These inhibitors are gating modifiers and are sensitive to channel activation.[11] For example, ProTx-II, a tarantula venom, was shown to selectively inhibit hNav1.7 with a half maximal inhibitory concentration (IC_{50}) of 0.3 nM, compared to values of 30−150 nM for other heterologously expressed Na_v1 subtypes.[12] A unique 46-residue peptide from centipede venom has also been identified. This potently and selectively inhibits $hNa_v1.7$ with an IC_{50} of ∼25 nM, compared to micromolar IC_{50} values for $hNa_v1.1$, $hNa_v1.2$, and $hNa_v1.6$ channels. It had no effect on $hNa_v1.3$, $hNa_v1.4$, $hNa_v1.5$, and $hNa_v1.8$.[9] Lee et al.[13] developed a monoclonal antibody that targets the voltage-sensor paddle of $hNa_v1.7$, effectively inhibiting the function of $hNa_v1.7$ in vitro with high specificity and potency (IC_{50} of 30.7 nM, with μM values for other Na_v channels). Klint et al.[14] reported the discovery of seven novel peptides from spider venom (NaSpTx family 1) which modulate the activity of $hNa_v1.7$. One of these toxins (rHd1a) was found to potently inhibit $hNa_v1.7$ (IC_{50} = 111 nM).[14] Recently, Focken et al.[15] discovered an aryl sulfonamide capable of immobilizing the voltage sensor of $hNa_v1.7$ with 0.4 nM binding affinity and selectivity over the cardiac ion channel $hNa_v1.5$. Moreover, they demonstrated in rodents that the compound had analgesic effects toward acute and inflammatory pain.

Inhibitors that potently block the selectivity filter of $hNa_v1.7$ may exhibit a more effective pain therapy, but only a small number exist.[4,17−19] An inhibitor capable of binding to the selectivity filter allows for binding to occur to all physiological channel states. For example, a recent study in humans demonstrated that the potent (IC_{50} of 80 nM) but nonselective $hNa_v1.7$ channel blocker XEN-402 significantly reduced the amount of pain experienced by patients when applied topically.[4] However, XEN-402 is not selective to $hNa_v1.7$ which limits its clinical use. Walker et al.[19] examined the binding of three toxins (tetrodotoxin, saxitoxin, and gonyautoxin), derived from pufferfish and paralytic shellfish, against primate $Na_v1.7$. They demonstrated that in primates, tetrodotoxin binds with high affinity to the $Na_v1.7$ ion channel while saxitoxin and gonyautoxin bind weakly. Using mutagenesis studies, Walker et al.[19] were able to highlight the importance of two ion channel residues, Thr-1398 and Ile-1399, as critical determinants of saxitoxin and gonyautoxin low affinity in $hNa_v1.7$. They suggest that selective inhibitors of $hNa_v1.7$ could be designed around these residues since in other hNa_v channels, the residues in equivalent positions occur as methionine and aspartate.

Many of the toxins extracted from venomous animals, such as cone snails and scorpions, have been identified as potent and specific inhibitors of voltage-gated cationic channels. Unfortunately, there are a number of challenges associated with converting toxins from venomous species to drugs, such as unstable disulfide bonds and susceptibility to protease degradation.[3,20−23] Although polypeptide toxins are unsuitable to be used as potential therapeutics due to their low stability in plasma and high cost of synthesis, they serve as useful structural templates for designing new therapeutic agents. Nanomaterials,[24] truncated peptides,[21] or peptidomimetic star polymers[25] designed to mimic the main features of these complex toxin structures may help to alleviate some of these challenges. Several previous studies[26−32] have shown that nanomaterials, such as carbon nanotubes and fullerenes, interact with certain classes of biological ion channels. We have demonstrated that a C_{84} fullerene with six lysine derivatives uniformly attached to its surface ($[Lys_6]$-C_{84} fullerene) can be a selective inhibitor of ion channels.[24] The lysine-decorated fullerene binds strongly (IC_{50} = 46 nM) to the bacterial sodium channel, Na_vAb, whereas it binds only weakly (IC_{50} = 3 mM) to the human voltage-gated potassium channel, $hK_v1.3$.[24] The stronger binding in the sodium channel was due to hydrophobic contacts with critical residues at the entrance to the Na_vAb pore.[24] The $[Lys_6]$-C_{84} fullerene was designed with the aim of mimicking the function of μ-conotoxins, derived from the marine cone snail, which bind with high affinity to the pore region of voltage-gated sodium channels (site 1 in Figure 1).[3,33] Of particular interest, two small μ-conotoxins, KIIIA and SIIIA, have been shown to have analgesic properties in mouse inflammatory pain assays.[3]

In this study, using molecular dynamics (MD) simulations, we investigate the sensitivity of $hNa_v1.7$ to the $[Lys_6]$-C_{84} fullerene as a possible drug lead for severe neuropathic pain. We also examine the potential of the fullerene derivative to bind to other human sodium ion channels isoforms.

■ RESULTS AND DISCUSSION

Configuration of the $hNa_v1.7$ and $hNa_v1.4$ Pore Domains. The pore domain of $hNa_v1.7$ and $hNa_v1.4$ are formed by four nonidentical subunits. The selectivity filter of $hNa_v1.7$ has a DEKA (Asp-Glu-Lys-Ala) ring, as opposed to the EEEE (Glu-Glu-Glu-Glu) ring found in the bacterial sodium channel Na_vAb. In our $hNa_v1.7$ and $hNa_v1.4$ models, one sodium ion is located in close proximity to the aspartate residue of the DEKA ring and acts to stabilize the pore. The distance from the sodium ion to the center of mass of the carboxyl group on the aspartate residue is measured to be 2.23 and 2.79 Å in our $hNa_v1.7$ and $hNa_v1.4$ models, respectively. The structure of the channel is stable, evidenced by the RMSD of the channel backbone fluctuating by only 1.67 Å with reference to the initial energy-minimized model (Figure S1 in the Supporting Information illustrates the RMSD during the unrestrained MD simulations).

Binding $[Lys_6]$-C_{84} Fullerene to $hNa_v1.7$ and $hNa_v1.4$. The PMF profiles for the cleavage of the $[Lys_6]$-C_{84} fullerene from $hNa_v1.7$ and $hNa_v1.4$ models are shown in Figure 2. The

DOI: 10.1021/acschemneuro.7b00099
ACS Chem. Neurosci. 2017, 8, 1747−1755

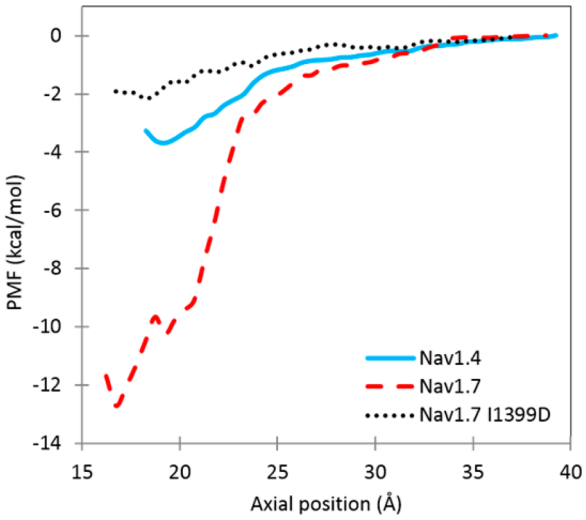

Figure 2. Potential of mean force for cleavage of [Lys$_6$]-C$_{84}$ fullerene from hNa$_v$1.7, hNa$_v$1.4, and hNa$_v$1.7 I1399D. The random errors of the PMF profiles estimated from the bootstrapping method[34,35] are less than 0.4 kcal/mol in all cases. Maximum uncertainty is estimated to be 0.04, 0.36, and 0.22 kcal/mol for the hNa$_v$1.7, hNa$_v$1.4, and mutant hNa$_v$1.7 I1399D models, respectively. The PMF of each channel is shown individually in Figure S2 in the Supporting Information to illustrate the binding pockets and error bars.

axial position is measured from the center of mass of the fullerene to the center of mass of each channel (in the z-direction). For hNa$_v$1.7, the PMF reaches a minimum (z_{min}) at 16.5 Å, with a well depth of −12.7 kcal/mol. In addition, a local minimum exists at 19.0 Å. For hNa$_v$1.4, the minimum (z_{min}) is located at 19.0 Å with a well depth of −3.7 kcal/mol. Using eq 1, we predict K_d values of 2.7 nM and 3.7 mM with negligible error for the hNa$_v$1.7 and hNa$_v$1.4 channels, respectively. The windows at 39.0 Å (hNa$_v$1.7) and 39.5 Å (hNa$_v$1.4) are assumed to be bulk (z_{max}), and the PMF is therefore set to zero at these z positions.

To characterize the interactions between the [Lys$_6$]-C$_{84}$ fullerene and the two channels, we examine the umbrella sampling window located at the PMF minima. The binding of the [Lys$_6$]-C$_{84}$ fullerene to hNa$_v$1.7 at 16.5 Å is illustrated in Figure 3. One fullerene-lysine side chain binds to Glu-916 and Glu-919 at the selectivity filter, forming an average of 0.5 ± 0.5 (mean ± standard deviation) and 0.7 ± 0.4 hydrogen bonds, respectively. Two other lysine residues attached to the fullerene bind to the channel Ser-279 and Asp-923 with an average of 0.2 ± 0.4 and 0.1 ± 0.4 hydrogen bonds, respectively. In addition, hydrophobic interactions occur between Ile-1399, Ile-1400, Leu-280 and Tyr-362 with the fullerene surface. (see Figures S3 and S4 in the Supporting Information which illustrate patterns of hydrogen bonding and hydrophobic interactions formed over the simulation time).

The binding of the [Lys$_6$]-C$_{84}$ fullerene to hNa$_v$1.4 at the minimum of the PMF is shown in Figure 4. We find that one lysine chain on the fullerene binds to Glu-409 and Asn-410 at the entrance to the selectivity filter, with an average of 0.6 ± 0.5 and 0.5 ± 0.5 hydrogen bonds, respectively. Another lysine chain of the [Lys$_6$]-C$_{84}$ fullerene binds to Asn-1226 in the outer vestibule with an average of 0.2 ± 0.4 hydrogen bonds (residue not shown in Figure 4). There are also three hydrophobic interactions formed between the fullerene surface and the residues Ile-1249, Ala-1252, and Ala-1253 (see Figures S3 and

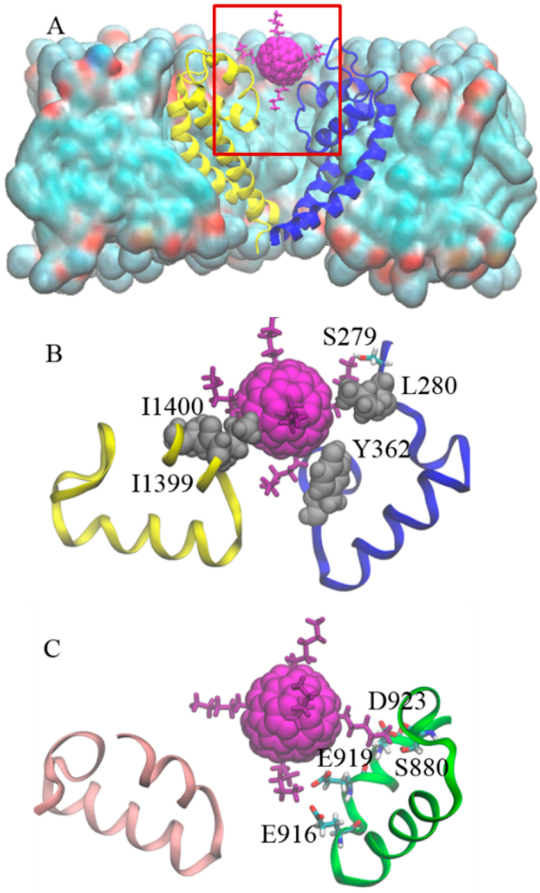

Figure 3. Binding of [Lys$_6$]-C$_{84}$ fullerene (purple) to the outer vestibule of hNa$_v$1.7 at 16.5 Å. (A) The entire channel embedded in the lipid bilayer. (B) and (C) illustrate detailed binding of the [Lys$_6$]-C$_{84}$ fullerene. For clarity, in (A) and (B), only domains I (blue) and III (yellow), and in (C) only domains II (green) and IV (pink) are shown. The hydrophobic residues Leu-280, Tyr-362, Ile-1399, and Ile-1400 are represented as silver van der Waals spheres. All other important residues (Ser-279, Ser-880, Glu-916, Glu-919, and Asp-923) are represented in licorice.

S4 in the Supporting Information which illustrate patterns of hydrogen bonding and hydrophobic interactions formed over the simulation time). As a result of these interactions the [Lys$_6$]-C$_{84}$ fullerene is positioned off-center and is not completely blocking the selectivity filter. It is not possible to undertake simulations for a long enough period of time to observe the passage of ions across the channel. The maximum distance between outermost atoms forming the channel pore is ∼11 Å at the location where the lysine chain is bound to Glu-409. Furthermore, the passage at this position is fully hydrated so that sodium ions under these conditions would readily move across the channel. A comparison of the solvent accessible volume between the hNa$_v$1.4 and hNa$_v$1.7 channels with the [Lys$_6$]-C$_{84}$ fullerene bound is shown in Figure 5.

Although hNa$_v$1.7 and hNa$_v$1.4 both exhibit a similar pattern of hydrogen bonding with the [Lys$_6$]-C$_{84}$ fullerene, an additional hydrophobic interaction occurs in the hNa$_v$1.7 model. It is of interest to determine how much this additional hydrophobic interaction may contribute to the free energy. Using density functional theory calculations, de Leon et al.[36,37] estimated the quantum mechanical gas phase interaction energy for the interaction of C$_{60}$ and C$_{80}$ with amino acids. We note

DOI: 10.1021/acschemneuro.7b00099
ACS Chem. Neurosci. 2017, 8, 1747−1755

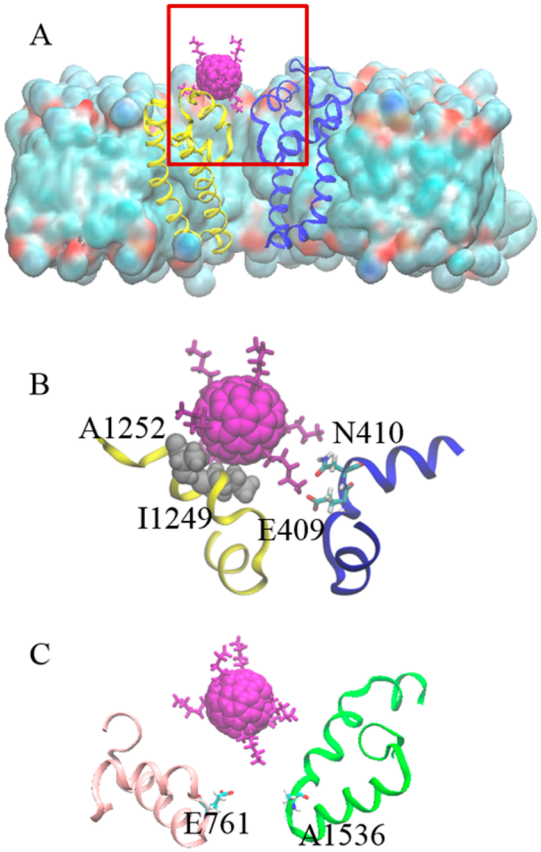

Figure 4. Binding of [Lys$_6$]-C$_{84}$ fullerene (purple) to the outer vestibule of hNa$_v$1.4 at 19.0 Å. (A) The entire channel embedded in the lipid bilayer. (B) and (C) illustrate detailed binding of the [Lys$_6$]-C$_{84}$ fullerene. For clarity, in (A) and (B), only domains I (blue) and III (yellow), and in (C) only domains II (pink) and IV (green) are shown. The hydrophobic residues Ala-1252 and Ile-1249 are represented as silver van der Waals spheres and Asn-410 and Glu-409 side chains are represented in licorice. For clarity, only a portion of the channel is shown.

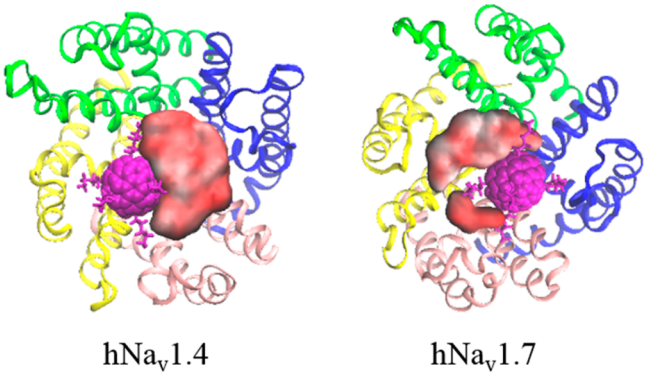

Figure 5. Solvent accessible volume of the hNa$_v$1.4 and hNa$_v$1.7 pore regions with the [Lys$_6$]-C$_{84}$ fullerene (purple) bound at 19.0 Å, and 16.5 Å, respectively. Domains I (blue), II (pink), III (yellow), and IV (green) are shown.

here that, since these values were measured in the gas phase they are likely to be different in our solvated model. de Leon et al.[36,37] determined interaction energies of alanine, isoleucine, tyrosine, and leucine residues from a C$_{80}$ fullerene as −4.853, −3.358, −6.492, and −5.933 kcal/mol, respectively.[37] Using these values, the combined interaction energy of the hydrophobic interactions formed between the [Lys$_6$]-C$_{84}$ fullerene and the hNa$_v$1.4 model (Ile-1249, Ala-1252 and Ala-1253) is ∼−13.064 kcal/mol. Similarly, the combined interaction energy of the hydrophobic interactions formed between the [Lys$_6$]-C$_{84}$ fullerene and the hNa$_v$1.7 model (Leu-280, Tyr-362, Ile-1399 and Ile-1400) is ∼−19.141 kcal/mol. Thus, the difference in interaction energy for the [Lys$_6$]-C$_{84}$ fullerene from the hydrophobic residues present at the entrance to the selectivity filter of hNa$_v$1.4 and hNa$_v$1.7 is −6.077 kcal/mol. This corresponds well to the difference in the depths of the two PMFs shown in Figure 2 (−9 kcal/mol).

As a local minimum also exists for hNa$_v$1.7 at 19.0 Å, the fullerene forms, on average, 1.1 ± 0.7 hydrogen bonds with hNa$_v$1.7 at this local minimum. Two lysine residues on the fullerene are bound to Glu-919 and Asp-1690 (see Figure 6) for an average of 81% and 24% of the entire simulation time, respectively.

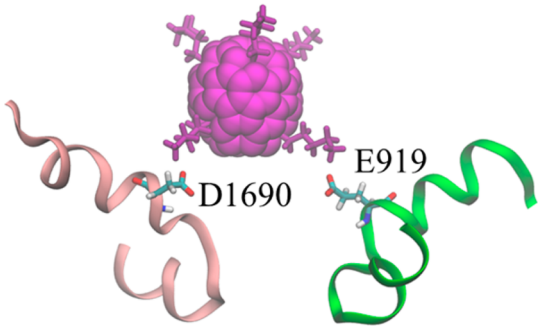

Figure 6. Binding of [Lys$_6$]-C$_{84}$ fullerene (purple) to the outer vestibule of hNa$_v$1.7 at the local minimum 19.0 Å. The side chains of residues Glu-919 and Asp-1690 are represented in licorice. Domains II and IV are shown in green and pink, respectively.

At positions corresponding to the methionine residues present in Na$_v$Ab and hK$_v$1.3,[24] hNa$_v$1.7 has residues Asn-Thr-Ile-Gly and hNa$_v$1.4 has residues Asn-Thr-Asp-Gly (see Table 1). In hNa$_v$1.7, the residue Ile-1399 forms a hydrophobic interaction with the fullerene surface, helping to coordinate it close to the pore. This is similar to the pattern of binding observed in the bacterial ion channel, Na$_v$Ab.[24] The lack of this stabilizing hydrophobic interaction and presence of a negative charge on the residue in the corresponding position, Asp-1248 in hNa$_v$1.4 results in a weaker interaction, shown by a much shallower well located further from the selectivity filter. This also precludes formation of hydrophobic interactions with otherwise nearby side chains.

Investigating a hNa$_v$1.7 Mutant. Since a small variation in sequence was shown to be so significant, we carried out an alignment of one representative of each of the 9 hNa$_v$ isoforms (see the Supporting Information for an alignment of one representative sequence from each of the 9 isoforms of hNa$_v$ channels). It can be clearly seen that an aspartate residue, rather than an isoleucine, occurs in all channels at the position corresponding to Ile-1399. To examine the effects of the aspartate residue on [Lys$_6$]-C$_{84}$ fullerene binding, we substitute an aspartate residue in hNa$_v$1.7 using computational mutagenesis as described in the Computational Methods section. Fullerene binding to the mutant was carried out as described for models hNa$_v$1.7 and hNa$_v$1.4. The PMF for cleavage of the fullerene from the mutant hNa$_v$1.7 (I1399D) reaches a minimum (z_{min}) at 18.5 Å with a well depth of −2.2 kcal/

DOI: 10.1021/acschemneuro.7b00099
ACS Chem. Neurosci. 2017, 8, 1747−1755

Table 1. Sequence Alignment of the Pore Regions of $hNa_v1.4$ and $hNa_v1.7$ Compared with the Region Surrounding the Selectivity Filter of the Homo-Tetrameric Channels, Na_vAb and $hK_v1.3$ (NCBI Reference 3RVY_A and NP_002223.3, Respectively)[a]

Ion channel	Continuous polypeptide sequence	Residue number
Na_vAb	FGTLGESFYTLFQVMTLESWSMGIVRPLMEVYPYAW	213
	*	
I $hNa_v1.7$	FDTFSWAFLALFRLMTQDYWENLYQQTLRAAGKTYM	379
$hNa_v1.4$	YDTFSWAFLALFRLMTQDYWENLFQLTLRAAGKTYM	424
	+ +	
II $hNa_v1.7$	MNDFFHSFLIVFRVLCGEWIETMWDCMEVAGQAMCLIV	936
$hNa_v1.4$	MHDFFHSFLIVFRILCGEWIETMWDCMEVAGQAMCLTV	781
	+ + -- +	
III $hNa_v1.7$	FDNVGLGYLSLLQVATFKGWTIIMYAAVDSVNVDKQPKYEYSL	1420
$hNa_v1.4$	YDNVGLGYLSLLQVATFKGWMDIMYAAVDSREKEEQPQYEVNL	1269
	+ ++ +++-------++	
IV $hNa_v1.7$	FETFGNSMICLFQITTSAGWDGLLAPILNSKPPDCD	1705
$hNa_v1.4$	FETFGNSIICLFEITTSAGWDGLLNPILNSGPPDCD	1554
	+ + + +	
$hK_v1.3$	SSIPDAFWWAVVTMTTVGYGDMHPVTIGGKIVGSLCA	465
	*	

[a]The alignment is generated using BLAST and CLUSTAL OMEGA 1.2.1 sequence alignment software.[45,46] The selectivity filter is highlighted in grey, acidic residues in red, basic residues in blue, and hydrophobic residues in green.[53] $hNa_v1.7$ residues that were substituted into $hNa_v1.4$ are indicated with a plus sign (+). Loop regions which were not modelled are indicated with a minus sign (−), and text in gray. Methionines interacting with the fullerene derivative (see text) are marked with an asterisk (*). Each domain of the hetero-tetrameric channels, $hNa_v1.4$ and $hNa_v1.7$ are indicated with roman numerals I−IV.

mol (see Figure 2). Using eq 1, we predict a K_d value of 14.5 mM for the mutant $hNa_v1.7$ (I1399D) channel. As previously, the window at 37.5 Å is assumed to be bulk (z_{max}), and the PMF is therefore set to zero at this z position. This result shows that the strength of binding is significantly reduced due to the mutation and instead, is of similar magnitude to that shown for binding the $[Lys_6]$-C_{84} fullerene to $hNa_v1.4$.

We find that three lysine chains on the fullerene bind to the mutant $hNa_v1.7$ (I1399D) channel. One lysine chain on the fullerene binds to Glu-919 and Asp-1399, with an average of 0.5 ± 0.5 and 0.3 ± 0.5 hydrogen bonds, respectively. Another lysine chain on the fullerene binds to Asn-282 and Glu-926, with an average of 0.2 ± 0.4 and 0.4 ± 0.5 hydrogen bonds, respectively. A third lysine chain on the fullerene binds to Glu-281 with an average of 0.4 ± 0.5 hydrogen bonds. There are also hydrophobic interactions being formed between the fullerene surface and the residue Leu-366. As the simulation progresses, the fullerene is pulled further off-center and the interaction with Leu-366 is lost. Hydrophobic interactions are then formed between the fullerene surface and the residues Ile-1400 and Ala-1694 (see Figures S3 and S4 in the Supporting Information which illustrate the patterns of hydrogen bonding and hydrophobic interactions formed over the simulation time).

Again, using the density functional theory calculations from de Leon et al.[36,37] the combined interaction energy of the hydrophobic interactions formed between the $[Lys_6]$-C_{84} fullerene and the mutant $hNa_v1.7$ (I1399D) model (Leu-366) is ∼ −5.933 kcal/mol. Thus, the difference in interaction energy for the $[Lys_6]$-C_{84} fullerene from the hydrophobic residues present at the entrance to the selectivity filter of $hNa_v1.7$ and the mutant $hNa_v1.7$ (I1399D) channels is −13.21 kcal/mol. This corresponds well to the difference in the depths of the two PMFs shown in Figure 2 (−10.5 kcal/mol). As the simulation progresses and the hydrophobic residues Ile-1400 and Ala-1694 replace the interaction with Leu-366 the difference in interaction energy becomes −10.93 kcal/mol, again comparing well with the difference in the depths of the two PMFs.

In conclusion, we have demonstrated selectivity of $hNa_v1.7$ over $hNa_v1.4$ in binding the $[Lys_6]$-C_{84} fullerene. We show that the $[Lys_6]$-C_{84} fullerene is capable of blocking the ion-conducting pathway of the voltage-gated sodium channel, $hNa_v1.7$ with strong affinity (2.7 nM). In contrast, the $[Lys_6]$-C_{84} fullerene binds only weakly to the mutant $hNa_v1.7$ (I1399D) (14.5 mM) and the sodium ion channel expressed in skeletal muscle, $hNa_v1.4$ (3.7 mM). A summary of the PMF minima and dissociation constants are given in Table 2.

Table 2. Values of z_{min}, z_{max}, PMF Minima, and K_d Values for the $hNa_v1.4$, $hNa_v1.7$ and Mutant $hNa_v1.7$ (I1399D) Models

model	z_{min} (Å)	z_{max} (Å)	PMF minima (kcal/mol)	K_d (nM)
$hNa_v1.4$	19.0	39.5	−3.7	3.7×10^6
$hNa_v1.7$	16.5	39.0	−12.7	2.7
mutant $hNa_v1.7$ (I1399D)	18.5	37.5	−2.2	14.5×10^6

Our simulations of $hNa_v1.4$ and $hNa_v1.7$ as well as $hNa_v1.7$ (I1399D) clearly identify Ile-1399 as a critical determinant in binding. Comparison of one representative from each of the nine human sodium channel isoforms shows that $hNa_v1.7$ is the only voltage-gated sodium channel where the outer ring charged aspartate in domain III is absent and occurs as a neutral isoleucine. Furthermore, the unique sequence of $hNa_v1.7$ is essential for selective binding of the $[Lys_6]$-C_{84} fullerene and subsequent blocking of the ion channel. Our results are consistent with findings by Walker and colleagues[19] who also identified hydrophobic interactions and Ile-1399 as a critical determinant for binding conotoxins.

Apart from one highly variable region around Ser-270 and Ser-280 in $hNa_v1.7$, the residues identified to be in close proximity to the bound $[Lys_6]$-C_{84} fullerene are nearly identical in all sodium channel isoforms other than $hNa_v1.7$. This

DOI: 10.1021/acschemneuro.7b00099
ACS Chem. Neurosci. 2017, 8, 1747−1755

suggests that the pattern of binding the [Lys_6]-C_{84} fullerene to other isoforms may be similar to the results obtained in binding the [Lys_6]-C_{84} fullerene to our $hNa_v1.4$ and $hNa_v1.7$ (I1399D) models. The binding to other isoforms will be investigated in ongoing research. Further studies will also be undertaken to explore alternative ion channel binding sites coupled with potential refinements to the fullerene derivative. The preliminary findings from this work confirm that the binding pocket created by select residues in the pore region of $hNa_v1.7$ is an optimal candidate site for investigating new sodium channel blockers for neuropathic pain relief.

■ COMPUTATIONAL METHODS

[Lys_6]-C_{84} Fullerene. The generation and optimization of the fullerene model is described in detail in our earlier paper.[24] Briefly, we generated the C_{84} fullerene (diameter approximately 8 Å) using the fullerene library available in Nanotube Modeler 1.7.3, with a D2d structure as this is the most commonly observed in experiments.[38,39] Then, using ArgusLab 4.0.1 we attached six lysine chains uniformly to the outside surface and geometry optimization was performed using default parameters, the Broyden−Fletcher−Goldfarb−Dhanno algorithm and the universal force field.[40]

Sodium Ion Channels. Models of the pore modules of three sodium ion channels, hNav1.4, hNav1.7, and mutant $hNa_v1.7$ (I1399D) are used in this study. The pore module is composed of the S5-P1-SF-P2-S6 structural elements from Domains I−IV which together form the outer vestibule and ion conductance pore of each channel (see the Supporting Information for alignments of the $hNa_v1.7$ and $hNa_v1.4$ channel sequences). The voltage sensor helices (S1−S4), cytoplasmic and extracellular loops are excluded from the models as they have been shown to not be involved in binding either the fullerene derivative[24] or μ-conotoxins on which the structure of the fullerene is based.[7,41,42] Including the voltage sensor domains, cytoplasmic and extracellular loop domains in our MD simulations would result in a large system and would be too computationally expensive.

Model of hNav1.4. The pore model of the human skeletal muscle sodium channel $hNa_v1.4$ has been well characterized.[43] Using MD simulations, the model was shown to transmit sodium ions in a pattern consistent with experimental data. It also contains a realistically positioned sodium ion within the selectivity filter of the channel. This model is kindly provided for this study by the authors.

Model of $hNa_v1.7$. A model of the human voltage-gated sodium channel $hNa_v1.7$ is generated from the 1977 amino acid sequence (NCBI Reference: NP_002968.1) by computational mutagenesis. The equilibrated $hNa_v1.4$ is used as a structural template.[43] We substitute residues from the $hNa_v1.7$ sequence using the inbuilt mutate plugin available in VMD 1.9.2.[49] The resulting model is optimized and refined during equilibration in the MD simulation in an explicit membrane-water system.

For this study, computational mutagenesis was possible due to (i) the high sequence identity between $hNa_v1.4$ and $hNa_v1.7$ (61% identity overall, increasing to 88% when limited to the P1-SF-P2 fullerene binding site,[45,46] see the Supporting Information for alignments of the $hNa_v1.7$ and $hNa_v1.4$ channel sequences), and (ii) residues being substituted into a well-studied model that was shown to conduct sodium ions. This approach resulted in a reliable structural model of $hNa_v1.7$. In contrast, in the absence of a high resolution eukaryotic ion channels crystal structure being yet available, and due to the low sequence similarity between the bacterial homotetrameric and eukaryotic heterotetrameric channel sequences (usually <25%), it can be difficult to generate conducting ion channel pore models de novo. Furthermore, optimizing structures with low sequence similarity involves extensive and prohibitively expensive computation for iterative model building and refinement that is not always successful. Since developing our $hNa_v1.7$ model the crystal structure of a eukaryotic voltage-gated sodium channel, Na_vPaS has become available.[5] We therefore compare our modeled structures to the Na_vPaS crystal structure to examine model quality.

Model of $hNa_v1.7$ (I1399D). A model of the $hNa_v1.7$ (I1399D) mutant is generated using the equilibrated $hNa_v1.7$ model as an initial structure. An aspartate amino acid is substituted for residue Ile1399 and the model is refined as described for the $hNa_v1.7$ model.

Model Quality. Most existing assessment programs are biased toward soluble, globular proteins for which a large number of crystal structures exist.[47] These programs are usually not suitable for analyzing membrane proteins. Therefore, evaluation of the quality of the $hNa_v1.7$ and $hNa_v1.7$ (I1399D) models is limited to visual inspection, stereochemistry analysis and comparison of superimposed models.

Visual inspection of models and assessment using embedded bioinformatics tools in protein visualizing programs SwissModel 4.1[48] and VMD 1.9.2[49] identified no prohibitive contacts within the models. Ramachandran analysis for stereochemical correctness was carried out using the program PROCHECK.[50,51] Results show that 99.4% of the backbone dihedral angles are within favored or allowed regions for the $hNa_v1.7$ model (see the Supporting Information). Only two residues were identified as having strained conformations: Ala-1333 and Leu-271. These residues are located in loops and turns at the membrane/extracellular interface of the ion channels and some flexibility in those regions is not unexpected. Results show that 100% of the backbone dihedral angles are within favored or allowed regions for the mutant hNav1.7 (I1399D) (see the Supporting Information) indicating that no conflicting contacts were introduced into the model as a result of the mutation. Root-mean-square-deviations (RMSD) on the superimposition of different regions of the backbone atoms of $hNa_v1.7$ and $hNa_v1.4$ models are between 1.6 Å (selectivity filter residues) and 2.4 Å (over all modeled regions). A comparison of $hNa_v1.7$ and mutant $hNa_v1.7$ (I1399D) backbone atoms showed RMSD values of between 2.1 Å (selectivity filter residues) and 2.5 Å (over all modeled regions).

A similar RMSD value of 2.6 Å was obtained when superimposing the α-carbon backbone atoms of the hNav1.7 model (over all modeled regions) on the recently determined Na_vPaS structure.[5] These results indicate strong similarity, both between our models and the solved structure.[52]

For ease of comparison between the bacterial and mammalian ion channels referred to in this study, sequence of residues surrounding the selectivity filter of $hNa_v1.4$ and $hNa_v1.7$ channels is extracted and aligned with corresponding Na_vAb and $K_v1.3$ sequences in Table 1. Coordinates of the $hNa_v1.7$ model are provided in the Supporting Information.

Molecular Dynamics Simulations. MD simulations are used to equilibrate the $hNa_v1.7$ model, determine the bound configuration of the [Lys_6]-C_{84} fullerene and calculate the potential of mean force (PMF) of the [Lys_6]-C_{84} fullerene binding to both $hNa_v1.7$ and $hNa_v1.4$. We use the equilibrated $hNa_v1.4$ model previously generated by Chen et al.[43] All MD simulations are performed using NAMD 2.10 and visualized using VMD 1.9.2.[44,49] Throughout, we use the CHARMM36 force field[54,55] and TIP3P water, with a time step of 2 fs, at constant pressure (1 atm), and temperature (310 K).

The $hNa_v1.7$ channel is embedded in a 3-palmitoyl-2-oleoyl-D-glycero-1-phosphatidylcholine (POPC) bilayer, solvated in approximately a 120 × 120 × 100 $Å^3$ box of water. Sodium and chloride ions are added to both neutralize the system and simulate a 250 mM ionic concentration. One sodium ion is placed within the selectivity filter to prevent the side chain of Lys-1395 reorientating and occluding the ion conduction pathway.[56] Initially, all atoms of the protein are fixed in position to allow the water and ions to equilibrate during the simulation period of approximately 0.1 ns. The entire system is then equilibrated for 20 ns with a harmonic restraint applied to the protein backbone. During this time, the inner cavity of the channel becomes hydrated. The hydrated protein is then equilibrated for a further 20 ns with all constraints removed.

The fullerene is then added to the system and initially placed near the entrance to the selectivity filter of the equilibrated protein at $z = 20$ Å, approximately 10 Å from the selectivity filter. All atoms of the protein and fullerene are fixed in position to allow the water and ions to equilibrate for a simulation period of 0.1 ns. Then the entire system

DOI: 10.1021/acschemneuro.7b00099
ACS Chem. Neurosci. 2017, 8, 1747−1755

is allowed to equilibrate for a further 10 ns with both the fullerene and protein unconstrained.

Umbrella Sampling. The PMF for the unbinding of the [Lys_6]-C_{84} fullerene from the $hNa_v1.4$ and $hNa_v1.7$ channels is determined using umbrella sampling.[57,58] Umbrella sampling windows are generated using steered MD simulations with a force constant of 30 kcal/mol/Å applied to pull the fullerene out of the binding site. During steered MD simulations the backbone atoms of the protein are fixed in position and a harmonic restraint of 0.2 kcal/mol/$Å^2$ is applied to all atoms of the [Lys_6]-C_{84} fullerene so that the fullerene structure is not significantly distorted during pulling. The harmonic restraint maintains the RMSD, with reference to the initial geometry optimized structure below 0.25 Å. The channel central axis (z-axis) is used as the reaction coordinate. Pulling generates a continuous number of configurations along the permeation pathway so that umbrella sampling windows can be constructed every 0.5 Å.

During umbrella sampling the center of mass of the backbone atoms of the fullerene is confined to be within a cylinder centered on the channel axis of radius (R) 15 and 20 Å for the $hNa_v1.4$ and $hNa_v1.7$ channels, respectively. Beyond this radius a harmonic potential of 20 kcal/mol/$Å^2$ is applied. The radius of the cylinder is chosen to balance two competing considerations: (1) to avoid excluding any interactions contributing to the binding process (R must be large), and (2) avoid making the sample space too large in order for the simulation to converge (R must be small).[59] As such, the radius (R) of the cylinder is different for $hNa_v1.4$ and $hNa_v1.7$. A force constant of 30 kcal/mol/$Å^2$ is applied in the z direction to constrain the center of mass of the fullerene to the sampling window. The center of mass coordinates of the fullerene is saved every 500 ps. The PMF is then constructed along the z direction using the weighted histogram analysis method.[34,35] Each sampling window is run for 8 ns. The PMF is shown to converge as the depth changes by 0.1 kcal/mol as the simulation time reaches 8 ns. Figure S5 in the Supporting Information illustrates the PMF convergence for the $hNa_v1.4$ model. A similar methodology was used to investigate the [Lys_6]-C_{84} fullerene with Na_vAb and $hK_v1.3$.[24]

The accuracy of the PMF is not only influenced by the accuracy of the force field and molecular models, systematic and random errors are also introduced during the simulation. Systematic error is largely influenced by the configuration space that is sampled during umbrella sampling simulations. However, the systematic error can only be estimated by comparing to experimentally predicted values which in this case is not possible. Random errors are also introduced when a PMF profile is generated from umbrella sampling simulations, but can be approximated using the bootstrapping method.[60] At each umbrella sampling window, we obtain a probability distribution of finding the fullerene at position z. We perform the bootstrapping method and generate 100 new random data sets according to the distribution produced by our simulations. We then estimate the uncertainty by comparing the PMFs calculated from these hypothetical trajectories or histograms as implemented by Grossfield.[35]

The entropic contributions of the fullerene and ion channel are implicitly taken into account in our PMF calculations, since we do not restrain the conformation of the [Lys_6]-C_{84} fullerene and the channel protein. Since the ligand and channel are fairly rigid in our simulation system, the entropic contributions are likely to be small.

The dissociation constant (K_d) in the unit of molar is estimated to be[24,59,61]

$$K_d^{-1} = 1000 N_A R^2 \int_{z_{min}}^{z_{max}} \exp(-W(z)/k_B T)\, dz \quad (1)$$

where $W(z)$ is the 1D PMF with the zero point located at the bulk, $1000N_A$ is used to convert from cubic meter to liter per mole, and k_B and T are Boltzmann's constant and temperature, respectively. Here, z_{min} is in the binding pocket and z_{max} is in the bulk. Table 2 outlines the values of z_{min} and z_{max} for the three models studied.

A hydrogen bond is assumed to be formed if the donor−acceptor distance is within 3.0 Å and the donor−hydrogen−acceptor angle is ≥150°. Hydrogen bonds are reported as an average over the entire simulation and the uncertainty is measured as the standard deviation. A hydrophobic interaction is assumed to be formed if any atom of a hydrophobic residue is within 4.0 Å of the fullerene surface.

■ ASSOCIATED CONTENT

Supporting Information

The Supporting Information is available free of charge on the ACS Publications website at DOI: 10.1021/acschemneuro.7b00099.

Atomic coordinates for the $hNa_v1.7$ structural model (PDB)

Alignment of $hNa_v1.7$ and $hNa_v1.4$ sodium ion channel sequences; Ramachandran analysis of the $hNa_v1.7$ structural model and the mutant $hNa_v1.7$ (I1399D) model; alignment of one representative sequence from each of the 9 isoforms of hNa_v channels; graphic representation of the total number of hydrogen bonds between the [Lys_6]-C_{84} fullerene and the $hNa_v1.4$, $hNa_v1.7$, and mutant $hNa_v1.7$ (I1399D) channels; graphic representation of the total number of hydrophobic interactions formed between the [Lys_6]-C_{84} fullerene and the $hNa_v1.4$, $hNa_v1.7$, and mutant $hNa_v1.7$ (I1399D) channels; RMSD of the protein backbone of the $hNa_v1.7$ model from the initial structure during the unrestrained molecular dynamics simulation; individual PMF profiles with error bars shown; PMF convergence for the $hNa_v1.4$ channel (PDF)

■ AUTHOR INFORMATION

Corresponding Author

*Mailing address: School of Chemical and Physical Sciences, Victoria University of Wellington, PO Box 600, Wellington 6140, New Zealand. E-mail: Tamsyn.Hilder@vuw.ac.nz.

ORCID

Tamsyn A. Hilder: 0000-0002-0267-2754

Author Contributions

A.R.: carried out the sequence analysis and model building. T.A.H.: conducted the MD simulations and analysis. All authors contributed to designing the project and writing the manuscript.

Funding

This work was supported by the Australian Research Council through a Discovery Early Career Researcher Award and the MAWA Trust. This work was supported by the NCI National Facility at the Australian National University.

Notes

The authors declare no competing financial interest.

■ ABBREVIATIONS

hNa_v, human voltage-gated sodium channel; MD, molecular dynamics; RMSD, root-mean-square-deviation; PMF, potential of mean force

■ REFERENCES

(1) King, G. F., and Vetter, I. (2014) No gain, no pain: $Na_v1.7$ as an analgesic target. *ACS Chem. Neurosci.* *5*, 749−751.

(2) Emery, E. C., Luiz, A. P., and Wood, J. N. (2016) $Na_v1.7$ and other voltage-gated sodium channels as drug targets for pain relief. *Expert Opin. Ther. Targets* *20*, 975−983.

(3) Knapp, O., McArthur, J. R., and Adams, D. J. (2012) Conotoxins targeting neuronal voltage-gated sodium channel subtypes: potential analgesics? *Toxins* *4*, 1236−1260.

DOI: 10.1021/acschemneuro.7b00099
ACS Chem. Neurosci. 2017, 8, 1747−1755

(4) de Lera Ruiz, M., and Kraus, R. L. (2015) Voltage-gated sodium channels: structure, function, pharmacology, and clinical indications. *J. Med. Chem. 58*, 7093−7118.
(5) Shen, H., Zhou, Q., Pan, X., Li, Z., Wu, J., and Yan, N. (2017) Structure of a eukaryotic voltage-gated sodium channel at near-atomic resolution. *Science 355*, eaal4326.
(6) Catterall, W. A. (2012) Voltage-gated sodium channels at 60: structure, function and pathophysiology. *J. Physiol. 590*, 2577−2589.
(7) Stevens, M., Peigneur, S., and Tytgat, J. (2011) Neurotoxins and their binding areas on voltage-gated sodium channels. *Front. Pharmacol. 2*, 71.
(8) Dib-Hajj, S. D., Yang, Y., Black, J. A., and Waxman, S. G. (2013) The Na(V)1.7 sodium channel: from molecule to man. *Nat. Rev. Neurosci. 14*, 49−62.
(9) Yang, S., Xiao, Y., Kang, D., Liu, J., Li, Y., Undheim, E. A. B., Klint, J. K., Rong, M., Lai, R., and King, G. F. (2013) Discovery of a selective NaV1.7 inhibitor from centipede venom with analgesic efficacy exceeding morphine in rodent pain models. *Proc. Natl. Acad. Sci. U. S. A. 110*, 17534−17539.
(10) Minett, M. S., Pereira, V., Sikandar, S., Matsuyama, A., Lolignier, S., Kanellopoulos, A. H., Mancini, F., Iannetti, G. D., Bogdanov, Y. D., Santana-Varela, S., Millet, Q., Baskozos, G., MacAllister, R., Cox, J. J., Zhao, J., and Wood, J. N. (2015) Endogenous opioids contribute to insensitivity to pain in humans and mice lacking sodium channel $Na_v1.7$. *Nat. Commun. 6*, 8967.
(11) Ahuja, S., Mukund, S., Deng, L., Khakh, K., Chang, E., Ho, H., Shriver, S., Young, C., Lin, S., Johnson, J. P., Jr., Wu, P., Li, J., Coons, M., Tam, C., Brillantes, B., Sampang, H., Mortara, K., Bowman, K. K., Clark, K. R., Estevez, A., Xie, Z., Verschoof, H., Grimwood, M., Dehnhardt, C., Andrez, J.-C., Focken, T., Sutherlin, D. P., Safina, B. S., Starovasnik, M. A., Ortwine, D. F., Franke, Y., Cohen, C. J., Hackos, D. H., Koth, C. M., and Payandeh, J. (2015) Structural basis of Nav1.7 inhibition by isoform-selective small-molecule antagonist. *Science 350*, aac5464.
(12) Schmalhofer, W. A., Calhoun, J., Burrows, R., Bailey, T., Kohler, M. G., Weinglass, A. B., Kaczorowski, G. J., Garcia, M. L., Koltzenburg, M., and Priest, B. T. (2008) Pro Tx-II, a selective inhibitor of NaV1.7 sodium channels, blocks action potential propagation in nociceptors. *Mol. Pharmacol. 74*, 1476−1484.
(13) Lee, J. H., Park, C. K., Chen, G., Han, Q., Xie, R. G., Liu, T., Ji, R. R., and Lee, S. K. (2014) A monoclonal antibody that targets a NaV1.7 channel voltage sensor for pain and itch relief. *Cell 157*, 1393−1404.
(14) Klint, J. K., Smith, J. J., Vetter, I., Rupasinghe, D. B., Er, S. Y., Senff, S., Herzig, V., Mobli, M., Lewis, R. J., Bosmans, F., and King, G. F. (2015) Seven novel modulators of the analgesic target Nav1.7 uncovered using a high-throughput venom-based discovery approach. *Br. J. Pharmacol. 172*, 2445−2458.
(15) Focken, T., Liu, S., Chahal, N., Dauphinais, M., Grimwood, M. E., Chowdhury, S., Hemeon, I., Bichler, P., Bogucki, D., Waldbrook, M., Bankar, G., Sojo, L. E., Young, C., Lin, S., Shuart, N., Kwan, R., Pang, J., Chang, J. H., Safina, B. S., Sutherlin, D. P., Johnson, J. P., Jr., Dehnhardt, C. M., Mansour, T. S., Oballa, R. M., Cohen, C. J., and Robinette, C. L. (2016) Discovery of aryl sulfonamides as isoform-selective inhibitors of $Na_v1.7$ with efficacy in rodent pain models. *ACS Med. Chem. Lett. 7*, 277−282.
(16) DiMauro, E. F., Altmann, S., Berry, L. M., Bregman, H., Chakka, N., Chu-Moyer, M., Bojic, E. F., Foti, R. S., Fremeau, R., Gao, H., Gunaydin, H., Guzman-Perez, A., Hall, B. E., Huang, H., Jarosh, M., Kornecook, T., Lee, J., Ligutti, J., Liu, D., Moyer, B. D., Ortuno, D., Rose, P. E., Schenkel, L. B., Taborn, K., Wang, J., Wang, Y., Yu, V., and Weiss, M. M. (2016) Application of a parallel synthetic strategy in the discovery of biaryl acyl sulfonamides as efficient and selective $Na_v1.7$ inhibitors. *J. Med. Chem. 59*, 7818−7839.
(17) Chowdhury, S., Chafeev, M., Liu, S., Sun, J., Raina, V., Chui, R., Young, W., Kwan, R., Fu, J., and Cadieux, J. A. (2011) Discovery of XEN907, a spirooxindole blocker of NaV1.7 for the treatment of pain. *Bioorg. Med. Chem. Lett. 21*, 3676−3681.
(18) Chakka, N., Bregman, H., Du, B., Nguyen, H. N., Buchanan, J. L., Feric, E., Ligutti, J., Liu, D., McDermott, J. S., Zou, A., McDonough, S. I., and Dimauro, E. F. (2012) Discovery and hit-to-lead optimization of pyrrolopyrimidines as potent, state-dependent $Na_v1.7$ antagonists. *Bioorg. Med. Chem. Lett. 22*, 2052−2062.
(19) Walker, J. R., Novick, P. A., Parsons, W. H., McGregor, M., Zablocki, J., Pande, V. S., and Du Bois, J. (2012) Marked difference in saxitoxin and tetrodoxin affinity for the human nociceptive voltage-gated sodium channel ($Na_v1.7$). *Proc. Natl. Acad. Sci. U. S. A. 109*, 18102−18107.
(20) Norton, R. S. (2010) μ−conotoxins as leads in the development of new analgesics. *Molecules 15*, 2825−2844.
(21) Khoo, K. K., Wilson, M. J., Smith, B. J., Zhang, M. M., Gulyas, J., Yoshikami, D., Rivier, J. E., Bulaj, G., and Norton, R. S. (2011) Lactam-stabilized helical analogues of the analgesic μ-conotoxin KIIIA. *J. Med. Chem. 54*, 7558−7566.
(22) Clark, R. J., Akcan, M., Kaas, Q., Daly, N. L., and Craik, D. J. (2012) Cyclization of conotoxins to improve their biopharmaceutical properties. *Toxicon 59*, 446−455.
(23) Dekan, Z., Vetter, I., Daly, N. L., Craik, D. J., Lewis, R. J., and Alewood, P. F. (2011) α-conotoxin ImI incorporating stable cystathionine bridges maintains full potency and identical three-dimensional structure. *J. Am. Chem. Soc. 133*, 15866−15869.
(24) Hilder, T. A., and Chung, S. H. (2013) Designing a C_{84} fullerene as a specific voltage-gated sodium channel blocker. *Nanoscale Res. Lett. 8*, 323.
(25) Chen, R., Lu, D., Xie, Z., Feng, J., Jia, Z., Ho, J., Coote, M. L., Wu, Y., Monteiro, M. J., and Chung, S. H. (2016) Peptidomimetic star polymers for targeting biological ion channels. *PLoS One 11*, e0152169.
(26) Park, K. H., Chhowalla, M., Iqbal, Z., and Sesti, F. (2003) Single-walled carbon nanotubes are a new class of ion channel blockers. *J. Biol. Chem. 278*, 50212−50216.
(27) Chhowalla, M., Unalan, H. E., Wang, Y., Iqbal, Z., Park, K., and Sesti, F. (2005) Irreversible blocking of ion channels using functionalized single-walled carbon nanotubes. *Nanotechnology 16*, 2982−2986.
(28) Xu, H., Bai, J., Meng, J., Hao, W., Xu, H., and Cao, J. M. (2009) Multi-walled carbon nanotubes suppress potassium channel activities in PC12 cells. *Nanotechnology 20*, 285102.
(29) Kraszewski, S., Tarek, M., Treptow, W., and Ramseyer, C. (2010) Affinity of C_{60} neat fullerenes with membrane proteins: a computational study on potassium channels. *ACS Nano 4*, 4158−4164.
(30) Monticelli, L., Barnoud, J., Orlowski, A., and Vattulainen, I. (2012) Interaction of C_{70} fullerene with the Kv1.2 potassium channel. *Phys. Chem. Chem. Phys. 14*, 12526−12533.
(31) Wong-Ekkabut, J., Baoukina, S., Triampo, W., Tang, I. M., Tieleman, D. P., and Monticelli, L. (2008) Computer simulation study of fullerene translocation through lipid membranes. *Nat. Nanotechnol. 3*, 363−368.
(32) Calvaresi, M., Furini, S., Domene, C., Bottoni, A., and Zerbetto, F. (2015) Blocking the passage: C_{60} geometrically clogs K^+ channels. *ACS Nano 9*, 4827−4834.
(33) Chen, R., and Chung, S. H. (2012) Binding modes of μ-conotoxin to the bacterial sodium channel (Na_vAb). *Biophys. J. 102*, 483−488.
(34) Kumar, S., Rosenberg, J. M., Bouzida, D., Swendsen, R. H., and Kollman, P. A. (1995) Multidimensional free-energy calculations using the weighted histogram analysis method. *J. Comput. Chem. 16*, 1339−1350.
(35) Grossfield, A. *WHAM: an implementation of the weighted histogram analysis method*, version 2.0.2, http://membrane.urmc.rochester.edu/content/wham/ (accessed August, 2008).
(36) de Leon, A., Jalbout, A. F., and Basiuk, V. A. (2008) Fullerene-amino acid interactions: a theoretical study. *Chem. Phys. Lett. 452*, 306−314.
(37) de Leon, A., Jalbout, A. F., and Basiuk, V. A. (2010) [80]Fullerene-amino acid interactions: theoretical insights. *Int. J. Quantum Chem. 110*, 953−959.

DOI: 10.1021/acschemneuro.7b00099
ACS Chem. Neurosci. 2017, 8, 1747−1755

(38) *JCrystalSoft: Nanotube modeller*, version 1.7.3. Copyright JCrystalSoft, 2005−2012 [http://www.jcrystal.com].
(39) Balch, A. L., Ginwalla, A. S., Lee, J. W., Noll, B. C., and Olmstead, M. M. (1994) Partial separation and structural characterization of C84 isomers by crystallization of (η^2-C_{84})Ir(CO)Cl(P-(C_6H_5)$_3$)$_2$. *J. Am. Chem. Soc. 116*, 2227−2228.
(40) *ArgusLab*, version 4.0.1, Mark Thompson and Planaria Software LLC, Copyright 1997−2004 [http://www.arguslab.com].
(41) Cusick, K. D., and Sayler, G. S. (2013) An overview on the marine neurotoxin, saxitoxin: genetics, molecular targets, methods of detection and ecological functions. *Mar. Drugs 11*, 991−1018.
(42) Cestèle, S., and Catterall, W. A. (2000) Molecular mechanisms of neurotoxin action on voltage-gated sodium channels. *Biochimie 82*, 883−892.
(43) Chen, R., Robinson, A., and Chung, S. H. (2014) Mechanism of μ-conotoxin PIIIA binding to the voltage-gated Na^+ channel $Na_v1.4$. *PLoS One 9*, e93267.
(44) Phillips, J. C., Braun, R., Wang, W., Gumbart, J., Tajkhorshid, E., Villa, E., Chipot, C., Skeel, R. D., Kale, L., and Schulten, K. (2005) Scalable molecular dynamics with NAMD. *J. Comput. Chem. 26*, 1781−1802.
(45) Sievers, F., Wilm, A., Dineen, D. G., Gibson, T. J., Karplus, K., Li, W., Lopez, R., McWilliam, H., Remmert, M., Söding, J., Thompson, J. D., and Higgins, D. G. (2011) Fast, scalable generation of high-quality protein multiple sequence alignments using Clustal Omega. *Mol. Syst. Biol. 7*, 539.
(46) Altschul, S. F., Madden, T. L., Schäffer, A. A., Zhang, J., Zhang, Z., Miller, W., and Lipman, D. J. (1997) Gapped BLAST and PSI-BLAST: a new generation of protein database search programs. *Nucleic Acids Res. 25*, 3389−3402.
(47) Studer, G., Biasini, M., and Schwede, T. (2014) Assessing the local structural quality of transmembrane protein models using statistical potentials (QMEANBrane). *Bioinformatics 30*, i505−i511.
(48) Guex, N., and Peitsch, M. C. (1997) SWISS-MODEL and the Swiss-PdbViewer: An environment for comparative protein modelling. *Electrophoresis 18*, 2714−2723.
(49) Humphrey, W., Dalke, A., and Schulten, K. (1996) VMD: visual molecular dynamics. *J. Mol. Graphics 14*, 33−38.
(50) Laskowski, R. A., Hutchinson, E. G., Michie, A. D., Wallace, A. C., Jones, M. L., and Thornton, J. M. (1997) PDBsum: a web-based database of summaries and analyses of all PDB structures. *Trends Biochem. Sci. 22*, 488−490.
(51) Laskowski, R. A., MacArthur, M. W., Moss, D. S., and Thornton, J. M. (1993) PROCHECK: a program to check the stereochemical quality of protein structures. *J. Appl. Crystallogr. 26*, 283−291.
(52) Chothia, C., and Lesk, A. M. (1986) The relation between the divergence of sequence and structure in proteins. *EMBO J. 5*, 823−826.
(53) Betts, M. J., and Russell, R. B. (2003) Amino acid properties and consequences of substitutions. In *Bioinformatics for Geneticists* (Barnes, M. R., and Gray, I. C., Eds.), pp 289−316, Wiley, Chichester.
(54) MacKerell, A. D., Jr., Feig, M., and Brooks, C. L., III (2004) Extending the treatment of backbone energetics in protein force fields: limitations of gas-phase quantum mechanics in reproducing protein conformational distributions in molecular dynamics simulations. *J. Comput. Chem. 25*, 1400−1415.
(55) MacKerell, A. D., Jr., Bashford, D., Bellott, M., Dunbrack, R. L., Jr., Evanseck, J. D., Field, M. J., Fischer, S., Gao, J., Guo, H., Ha, S., Joseph-McCarthy, D., Kuchnir, L., Kuczera, K., Lau, F. T., Mattos, C., Michnick, S., Ngo, T., Nguyen, D. T., Prodhom, B., Reiher, W. E., Roux, B., Schlenkrich, M., Smith, J. C., Stote, R., Straub, J., Watanabe, M., Wiórkiewicz-Kuczera, J., Yin, D., and Karplus, M. (1998) All-atom empirical potential for molecular modeling and dynamics studies of proteins. *J. Phys. Chem. B 102*, 3586−3616.
(56) Xia, M., Liu, H., Li, Y., Yan, N., and Gong, H. (2013) The mechanism of Na^+/K^+ selectivity in mammalian voltage-gated sodium channels based on molecular dynamics simulation. *Biophys. J. 104*, 2401−2409.
(57) Torrie, G. M., and Valleau, J. P. (1977) Nonphysical sampling distributions in Monte Carlo free energy estimation: Umbrella sampling. *J. Comput. Phys. 23*, 187−199.
(58) Roux, B. (1995) The calculation of the potential of mean force using computer simulations. *Comput. Phys. Commun. 91*, 275−282.
(59) Gordon, D., Chen, R., and Chung, S. H. (2013) Computational methods of studying the binding of toxins from venomous animals to biological ion channels: theory and applications. *Physiol. Rev. 93*, 767−802.
(60) Zhu, F., and Hummer, G. (2012) Convergence and error estimation in free energy calculations using the weighted histogram analysis method. *J. Comput. Chem. 33*, 453−465.
(61) Allen, T. W., Andersen, O. S., and Roux, B. (2004) Energetics of ion conduction through the gramicidin channel. *Proc. Natl. Acad. Sci. U. S. A. 101*, 117−122.

DOI: 10.1021/acschemneuro.7b00099
ACS Chem. Neurosci. 2017, 8, 1747−1755